

1 **SUPPORTING INFORMATION**

2 **Cluster Dynamics-based Parameterization for Sulfuric Acid-Dimethylamine**
3 **Nucleation: Comparison and Selection through Box- and Three-Dimensional-**
4 **Modeling**

5
6 Jiewen Shen^{1,2}, Bin Zhao^{1,2}, Shuxiao Wang^{1,2,*}, An Ning³, Yuyang Li², Runlong Cai⁴,
7 Da Gao^{1,2}, Biwu Chu^{5,6}, Yang Gao⁷, Manish Shrivastava⁸, Jingkun Jiang², Xiuhui
8 Zhang³, Hong He^{5,6}

9
10 ¹*State Key Joint Laboratory of Environment Simulation and Pollution Control, School*
11 *of Environment, Tsinghua University, Beijing, 100084, China*

12 ²*State Environmental Protection Key Laboratory of Sources and Control of Air*
13 *Pollution Complex, Beijing, 100084, China*

14 ³*Key Laboratory of Cluster Science, Ministry of Education of China, School of*
15 *Chemistry and Chemical Engineering, Beijing Institute of Technology, Beijing, 100081,*
16 *China*

17 ⁴*Shanghai Key Laboratory of Atmospheric Particle Pollution and Prevention (LAP³),*
18 *Department of Environmental Science & Engineering, Fudan University, Shanghai,*
19 *200438, China*

20 ⁵*State Key Joint Laboratory of Environment Simulation and Pollution Control,*
21 *Research Center for Eco-Environmental Sciences, Chinese Academy of Sciences,*
22 *Beijing 100085, China*

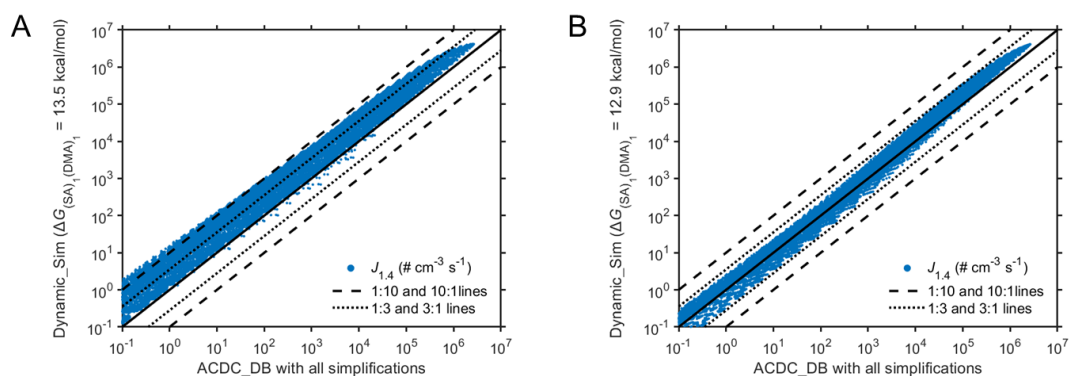
23 ⁶*College of Resources and Environment, University of Chinese Academy of Sciences,*
24 *Beijing 100049, China*

25 ⁷*Key Laboratory of Marine Environment and Ecology, Ministry of Education, Ocean*
26 *University of China, Qingdao 266100, China*

27 ⁸*Pacific Northwest National Laboratory, Richland, Washington, USA*

28
29 * Correspondence to: Shuxiao Wang (shxwang@tsinghua.edu.cn)

30
31 *Totally 11 Figures and 2 Tables*
32



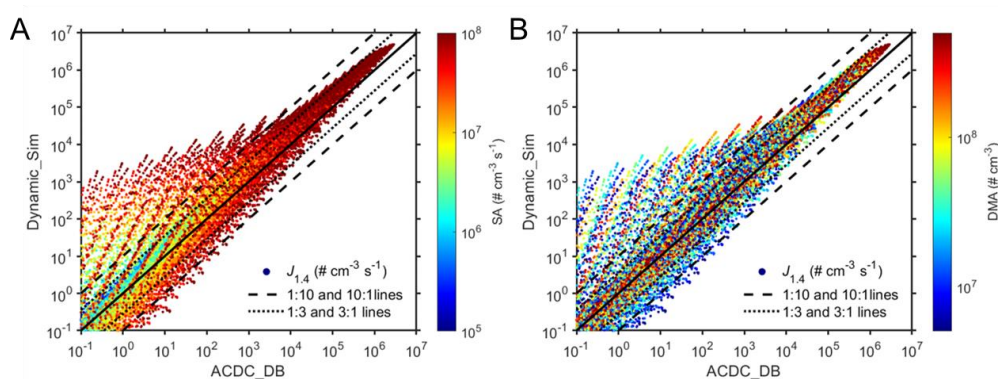
34

35

36 **Figure S1.** Comparison of $J_{1,4}$ predictions between ACDC_DB with all simplifications
 37 and Dynamic_Sim with different ΔG for initial $(SA)_1(DMA)_1$ cluster. A: $\Delta G = 13.5$
 38 kcal/mol; B: $\Delta G = 12.9$ kcal/mol (Ning et al. 2024). Solid dots represent simulated $J_{1,4}$
 39 values, solid lines indicate a 1:1 line, dotted lines correspond to 1:3 and 3:1 lines, and
 40 dashed lines represent 1:10 and 10:1 lines.

41

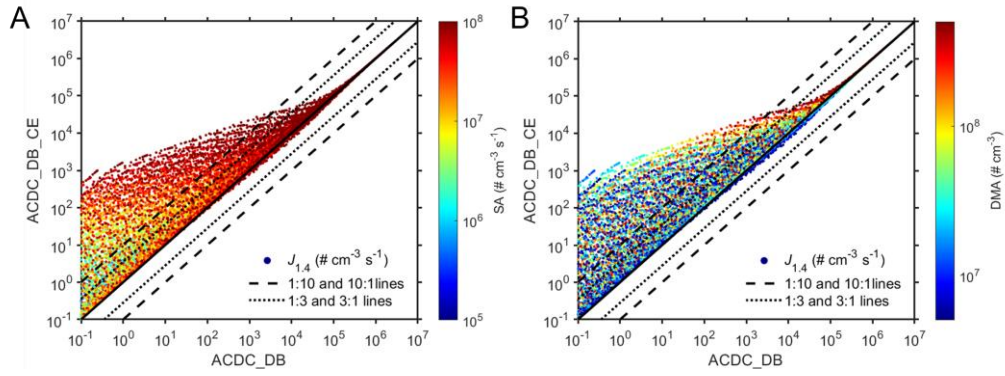
42



43

44 **Figure S2.** Comparison of $J_{1,4}$ predictions between ACDC_DB and Dynamic_Sim
 45 correlated with $[SA]$ variation (A) and $[DMA]$ variation (B). Solid dots represent
 46 simulated $J_{1,4}$ values, solid lines indicate a 1:1 line, dotted lines correspond to 1:3 and
 47 3:1 lines, and dashed lines represent 1:10 and 10:1 lines.

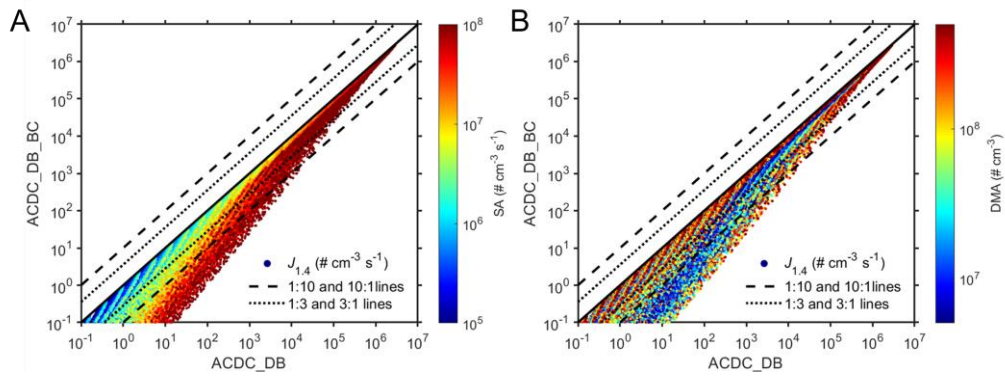
48



49

50 **Figure S3.** Same as Figure S2 but for ACDC_DB_CE.

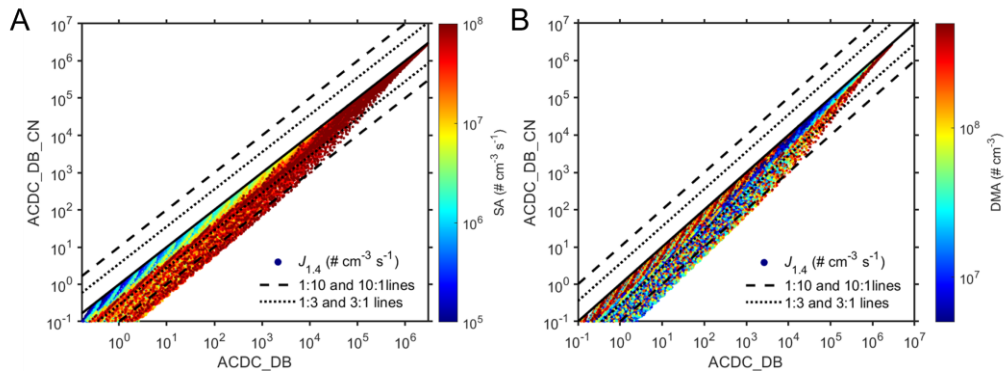
51



52

53 **Figure S4.** Same as Figure S2 but for ACDC_DB_BC.

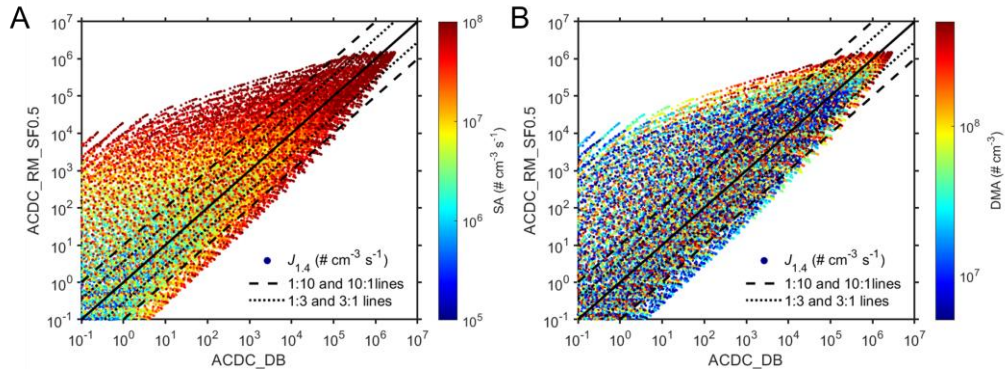
54



55

56 **Figure S5.** Same as Figure S2 but for ACDC_DB_CN.

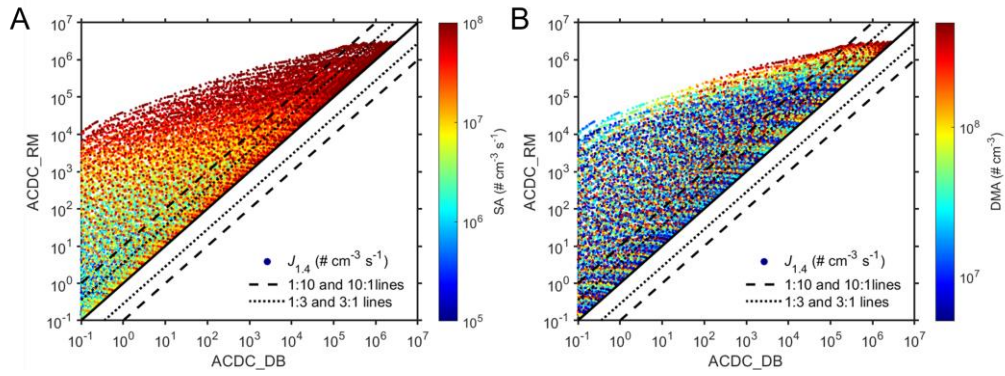
57



58

59 **Figure S6.** Same as Figure S2 but for ACDC_RM_SF0.5.

60

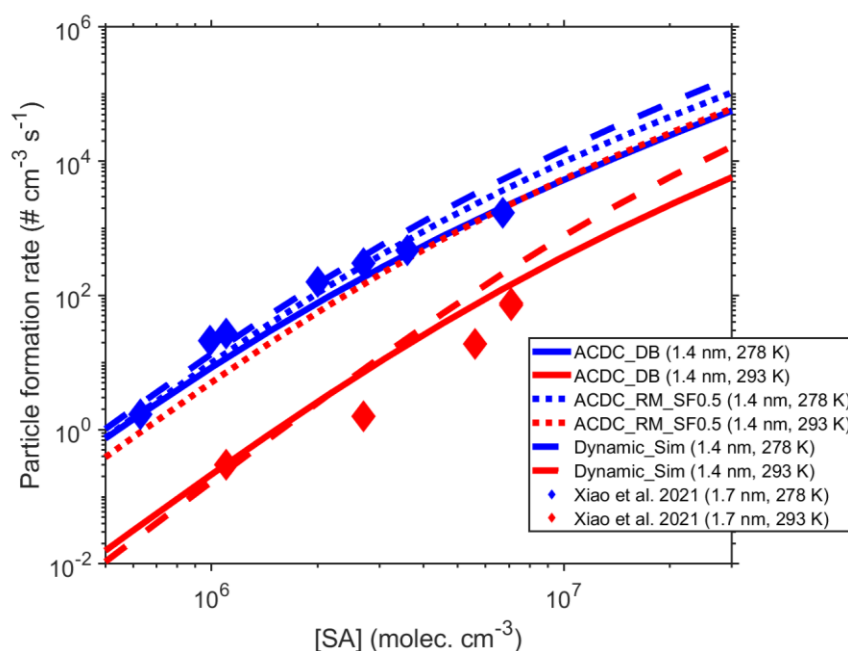


61

62 **Figure S7.** Same as Figure S2 but for ACDC_RM.

63

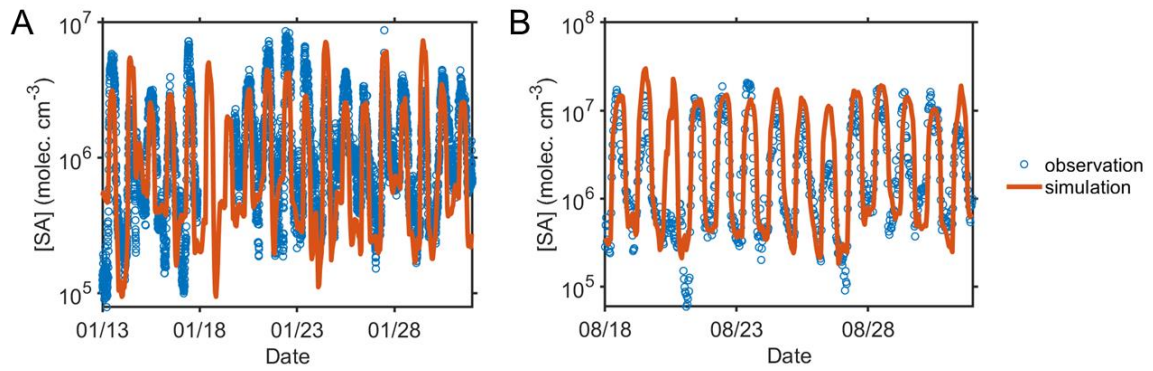
64



66

67 **Figure S8.** Comparison of modeled particle formation rates with measurements from
 68 CLOUD chamber experiments conducted by Xiao et al. 2021. Blue lines or diamonds
 69 represent particle formation rates at 278 K, while red ones represent those at 293 K;
 70 solid, dotted, and dashed lines denote the simulated results of ACDC_DB,
 71 ACDC_RM_SF0.5, and Dynamic_Sim, respectively. The simulations were conducted
 72 following the experimental conditions of Xiao et al. 2021, with specific conditions
 73 provided in their Table S1 and Table S2. It is noteworthy that Xiao et al. 2021 reported
 74 particle formation rates at 1.7 nm, whereas our simulations are at 1.4 nm. This
 75 discrepancy may lead to a slight overestimation of the simulated particle formation rates
 76 for simulations compared to the experiments. However, in the experiments, ~1 ppbv
 77 NH₃ was involved besides DMA during nucleation, which might enhance nucleation
 78 rates somewhat even through DMA is the dominant enhancing agent for SA-driven
 79 nucleation. Therefore, the two effects could partly offset each other, allowing for a
 80 direct comparison of particle formation rates between simulations and measurements.

81

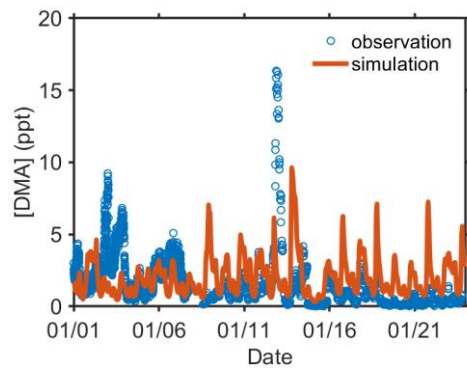


82

83 **Figure S9.** Comparison of simulated and observed SA concentrations. A for January
 84 and B for August 2019.

85

86



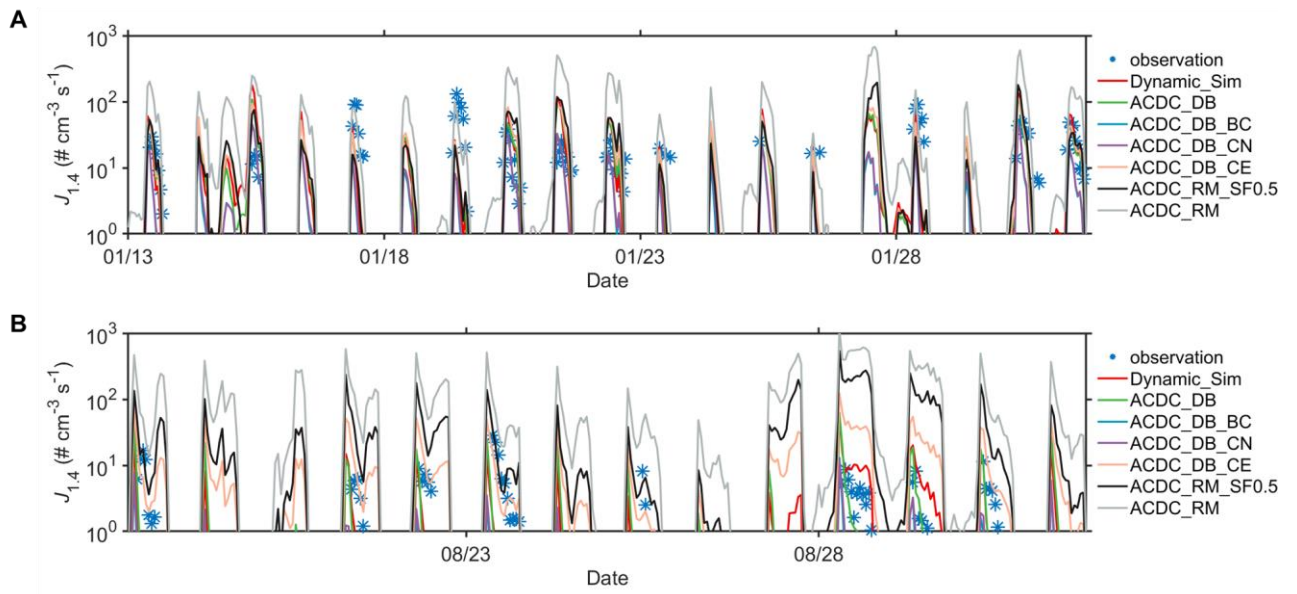
87

88 **Figure S10.** Comparison of simulated and observed DMA concentrations in January
 89 2019. Only data for winter month (January 2019) is available.

90

91

92



93
 94 **Figure S11.** Comparison of simulated particle formation rates with those derived from
 95 field measurements during (A) January 13, 2019, to January 31, 2019, and (B) August
 96 18, 2019, to August 31, 2019, in Beijing.

97
 98
 99
 100

101 **Table S1.** The ranges, total numbers and values at each point for the input parameters
 102 in deriving look-up tables

	Range	Number of points	Values at each point
T (K)	250 – 320	15	$250 + 5 \times i, i = 1, 15$
CS (s^{-1})	$5 \times 10^{-4} - 5 \times 10^{-1}$	16	$5 \times 10^{-4} \times 10^{0.2 \times i}, i = 1, 16$
[SA] ($\# \text{ cm}^{-3}$)	$1 \times 10^5 - 1 \times 10^8$	16	$1 \times 10^5 \times 10^{0.2 \times i}, l = 1, 16$
[DMA] ($\# \text{ cm}^{-3}$)	$5 \times 10^6 - 1 \times 10^8$	11	$5 \times 10^6 \times 10^{0.2 \times i}, i = 1, 11$

103

104

105

106

107 **Table S2.** Comparison of simulated and observed concentrations of the nucleating
 108 precursors.

Precursor	Time period	Site	Simulation	Observation	Bias	NMB
SA ($\#/\text{cm}^3$)	2019.01.13- 2019.01.31	Beijing	1.35×10^6	1.47×10^6	1.20×10^5	-10.80%
	2019.08.18- 2019.08.31		5.74×10^6	3.51×10^6	2.23×10^6	14.32%
DMA (pptv)	2019.01.01- 2019.01.31	Beijing	1.96	1.98	-0.02	-10.96%

109

110

111 **REFERENCES**

112 Xiao, M., Hoyle, C. R., Dada, L., Stolzenburg, D., Kürten, A., Wang, M.,
113 Lamkaddam, H., Garmash, O., Mentler, B., Molteni, U., Baccharini, A., Simon,
114 M., He, X.-C., Lehtipalo, K., Ahonen, L. R., Baalbaki, R., Bauer, P. S., Beck,
115 L., Bell, D., Bianchi, F., Brilke, S., Chen, D., Chiu, R., Dias, A., Duplissy, J.,
116 Finkenzeller, H., Gordon, H., Hofbauer, V., Kim, C., Koenig, T. K.,
117 Lampilahti, J., Lee, C. P., Li, Z., Mai, H., Makhmutov, V., Manninen, H. E.,
118 Marten, R., Mathot, S., Mauldin, R. L., Nie, W., Onnela, A., Partoll, E., Petäjä,
119 T., Pfeifer, J., Pospisilova, V., Quéléver, L. L. J., Rissanen, M., Schobesberger,
120 S., Schuchmann, S., Stozhkov, Y., Tauber, C., Tham, Y. J., Tomé, A., Vazquez-
121 Pufleau, M., Wagner, A. C., Wagner, R., Wang, Y., Weitz, L., Wimmer, D., Wu,
122 Y., Yan, C., Ye, P., Ye, Q., Zha, Q., Zhou, X., Amorim, A., Carslaw, K.,
123 Curtius, J., Hansel, A., Volkamer, R., Winkler, P. M., Flagan, R. C., Kulmala,
124 M., Worsnop, D. R., Kirkby, J., Donahue, N. M., Baltensperger, U., El
125 Haddad, I., and Dommen, J.: The driving factors of new particle formation and
126 growth in the polluted boundary layer, *Atmospheric Chemistry and Physics*,
127 21, 14275-14291, 10.5194/acp-21-14275-2021, 2021.

128

129